Red Light Phototherapy Using Light-Emitting Diodes Inhibits Melanoma Proliferation and Alters Tumor Microenvironments

Evan Austin[1,2], Alisen Huang[1], Jennifer Y. Wang[1], Marc Cohen[1], Edward Heilman[1], Emanual Maverakis[2], Josef Michl[3] and Jared Jagdeo[1,2]*

[1] Department of Dermatology, State University of New York (SUNY) Downstate Medical Center, Brooklyn, NY, United States,
[2] Department of Dermatology, University of California (UC) Davis Medical Center, Sacramento, CA, United States,
[3] Department of Pathology, SUNY Downstate Medical Center, Brooklyn, NY, United States

Background: Total annual cancer rates have decreased due to improved treatment and prevention. However, the incidence of melanoma is rising, and not all patients respond to immune and targeted approaches. Therefore, we sought to determine the efficacy of red light (RL) phototherapy in preclinical models of melanoma.

Methods: Melanoma cells (A375, B16F10, MNT-1) were irradiated with RL. Melanoma proliferation, apoptosis, oxidative stress, and p53 phosphorylation were measured *in vitro*. In C57BL/6 mice, phototherapy safety, B16F10 tumor growth, and immunocyte infiltration were assessed following RL.

Results: *In vitro*, 640 J/cm^2 RL decreased cellular proliferation without increasing apoptosis, while 1280 J/cm^2 increased apoptosis. RL increased intracellular reactive oxygen species generation and p53 phosphorylation. In animal models, 2560 J/cm^2 RL significantly prevented melanoma growth and increased the expression of CD103+ dendritic cells. 1280 and 1920 J/cm^2 RL decreased tumor volume, but not significantly. RL did not cause skin inflammation or erythema in normal skin.

Conclusion: RL represents a potentially safe and effective melanoma therapeutic. RL prevented tumor growth and increased the expression of immune markers, such as CD103, that are associated with favorable melanoma outcomes. Further research is needed to determine the optimal clinical treatment regimen for melanoma using RL.

Keywords: melanoma, phototherapy, low level light therapy, photobiomodulation therapy, reactive oxygen species, tumor micro environment

Abbreviations: ABAM, Antibiotic-antimycotic mixture; ANOVA, Analysis of variance; CPD, Cyclobutane pyrimidine dimer; DHR-123, Dihydrorhodamine-123; FBS, Fetal bovine serum; HDF, Human dermal fibroblasts; IHC, Immunohistochemistry; LED, Light-emitting diode; MFI, Median fluorescence intensity; NAC, N-acetylcysteine; OD, Optical density; RL, Red light; ROS, Reactive oxygen species; 7-AAD, 7-Aminoactinomycin D.

INTRODUCTION

While overall yearly cancer rates have decreased due to improved identification and prevention, the incidence of melanoma is increasing (1–3). For primary melanomas (Stage I and II), surgery is usually recommended with margins up to 2 cm (4, 5). Treatments for metastatic melanoma include immune modulators, kinase (i.e., targeted) inhibitors, and radiation therapy (5). Immune checkpoint inhibitors and kinase inhibitors may improve overall survival in up to 50% of patients (6). Despite improvements in outcomes, patients may have or develop resistance to kinase and immune checkpoint inhibitors (5). To improve efficacy, immune checkpoint inhibitors have been used in combination with radiation therapy *via* abscopal effects (7, 8).

Red light (RL) phototherapy may also be a beneficial adjunctive melanoma therapy by inhibiting tumor growth and augmenting anti-tumor immune activity. RL may non-thermally alter cellular biology *via* a process termed photobiomodulation (9). RL absorption by cytochrome c oxidase, a photoreceptive chromophore, excites electrons, activates the electron transport chain, and generates second messengers such as reactive oxygen species (ROS) (9, 10). Cancers, including melanoma, have dysregulated ROS homeostasis and may be particularly sensitive to oxidative stress (9, 11). Increasing intracellular ROS in cancer cells may lead to cell death or inhibition of growth and metastasis (12–14). Herein, we assessed the efficacy of RL phototherapy as a treatment for melanoma using translational models. *In vitro*, RL decreased melanoma cell proliferation and increased apoptosis, oxidative stress, and p53 phosphorylation. In mouse models, RL decreased melanoma tumor growth and increased the association of immune markers related to beneficial tumor immune microenvironments.

MATERIALS AND METHODS

Cell Culture

Monolayers of A375 (ATCC), B16F10 (ATCC), and MNT-1 (ATCC) melanoma cells were cultured in DMEM (Thermo Fisher) with 10% fetal bovine serum (FBS) and 1% Antibiotic-antimycotic mixture (ABAM). Cell cultures were maintained in a humidified incubator at 37°C with 5% carbon dioxide and atmospheric oxygen. For experiments, cells were seeded at low confluency (4,000 cells per 1.77 cm^2 surface area) (15). Twenty-four hours after plating, melanoma cells were irradiated with RL. **Supplemental Table 1** includes descriptions of the A375, MNT-1, and B16F10 cell lines.

In Vitro Irradiation

Melanoma cells were irradiated with an RL array (633 ± 15-nm, 87 mW/cm^2 at the light-emitting diode (LED) array surface, Omnilux Revive 2) at 640 and 1280 J/cm^2. Cells receiving 640 and 1280 J/cm^2 RL were irradiated outside the incubator for 2 and 4 hours (media temperature 34°C). Each RL-treated group was compared to a temperature, humidity, and CO_2 matched control group on a heating block (34°C). The time-matched controls for 640 and 1280 J/cm^2 are 2H (2 hours) and 4H (4 hours) controls, respectively.

Experimental irradiations were performed with DMEM (Thermo Fisher) supplemented with FBS and ABAM but without phenol red. Phenol red may alter antioxidant capacity, and thereby confound experiments (16). Additionally, A375 cells were cultured in CO_2-independent media to assess the effect of media pH on our findings (**Supplemental Methods**). Similar findings were observed when A375 cells were cultured in DMEM or CO_2-independent media, suggesting the results were not due to environmental conditions during treatment (**Supplemental Figure 1**).

Crystal Violet Cell Count

Cell counts were assessed using crystal violet (Thermo Fisher) (17, 18). Following treatment with RL, experimental and control samples were incubated for 48 hours to allow cell growth. Collected cells were fixed with 4% formaldehyde (Thermo Fisher) and stained with 0.1% crystal violet. Crystal violet was eluted with 10% acetic acid (Sigma), and optical density (OD) was quantified with a Biotek plate reader at 590-nm. Relative cell count was determined by comparing the OD of the RL and control samples.

Trypan Blue Cell Count and Viability

48 hours after RL irradiation, cell counts were assessed with a hemocytometer, according to previous protocols (19).

Cell Cycle Analysis

Cell cycle distribution was assayed using propidium iodide flow cytometry according to previously published protocols (20, 21). 24 hours after plating, A375 and MNT-1 cells were serum-starved (0% FBS) for 24 hours, then irradiated with RL. Fluorescent intensity was then immediately analyzed with flow cytometry (BD Fortessa). Cell cycle distribution was determined with Flowjo software using the Watson pragmatic algorithm (BD Biosciences).

Apoptosis/Necrosis

Annexin-V and 7-aminoactinomycin D (7-AAD; Sigma Millipore) were used to assay apoptosis/necrosis 24 hours post-RL irradiation using flow cytometry according to the manufacturer's recommendation (20, 22). Gating was assessed using a positive control sample heated at 70°C for 10 mins before annexin-v and 7-AAD staining. *Post-hoc* gating and analysis were performed with Flowjo software.

Free Radical Reactive Oxygen Species (ROS) Generation

Melanoma cells were assayed using DHR-123 at 0 hours post-RL irradiation (23). Cells were irradiated with RL and then stained with 1 ml of 1:100 DHR-123 (Thermo Fisher). Non-fluorescent DHR-123 converts to fluorescent rhodamine-123 in the presence of ROS. Rhodamine-123 median fluorescent intensity (MFI) was quantified with flow cytometry. *Post-hoc* gating and analysis were performed with Flowjo software.

DNA Damage

DNA from cells was collected (Qiagen FlexiGene DNA isolation kit) at 0 or 3 hours following RL or 10 J/cm^2 of UVB (positive

control) irradiation. DNA was then collected according to the manufacturer's recommendation. DNA quantity and quality were measured with a Nanodrop (Thermo Fisher). CPDs were quantified using ELISA according to the manufacturer's protocols (Cellbiolabs) with a plate reader at 405-nm.

Antioxidant Pretreatments

Cells were pretreated with 0.25 to 7.5 mM NAC (Sigma), a free radical scavenger, in DMEM for 2 hours to assess ROS-mediated pathways. Following antioxidant treatment, the cells were washed and fresh culture media was added. The cells were then irradiated with 640 J/cm^2 RL. 48 hours following RL treatment, changes in cell proliferation were assessed using crystal violet as described above.

Protein Collection and Western Blot

Protein was collected from RL treated and control cells 24 hours post-irradiation. Western blot was performed according to the manufacturer's protocols (**Supplemental Methods**).

Mouse Care and Use

C57BL/6 mice were housed and cared for in the animal facility in the Department of Comparative Medicine at SUNY Downstate (IACUC ID: 19-10564). Animals were provided a standard chow diet and always had full access to food and water.

Mouse Irradiations

Female C57BL/6 mice were irradiated daily with RL phototherapy (633 ± 15-nm, Omnilux Revive 2) at a power density of 87 mW/cm^2. Mice were treated in custom-designed temperature-controlled treatment cages to prevent supraphysiologic temperatures from the RL array and light (**Supplemental Figure 2**). Daily treatment regimens were 1280, 1920, and 2560 J/cm^2 which corresponded to 4 hours (4H), 6 hours (6H), and 8 hours (8H) of RL treatment, respectively. The ambient temperature in the cages was maintained using a temperature probe in the cage and air-conditioning unit. Mouse core body temperature was maintained between 34.5 and 38.9°C measured using a rectal temperature probe.

Safety Regimen

On day 0, the backs of the female C57BL/6 mice were shaved and naired while anesthetized with inhaled isoflurane. On day 1, 3 mice were randomly allocated to each control or RL treatment (daily 1280, 1920, or 2560 J/cm^2) group (n=3). On days 1-15, the mice received daily irradiations of 1280, 1920, or 2560 J/cm^2. During daily RL treatments, the mice were observed for changes in behavior, and rectal temperatures were recorded. On day 16, the mice were euthanized. Skin sections were fixed in 10% formalin and processed for IHC.

Efficacy Regimen

RL efficacy was assessed in female C57BL/6 mice injected with 3 x 10^5 B16F10 cells. Starting on day 3, the mice received daily irradiations of 1280 (n=10), 1920 (n=10), or 2560 J/cm^2 (n=12). To prevent overcrowding during the treatment protocol, the 1280, 1920, and 2560 J/cm^2 treatment regimens were performed separately with an equal number of control mice (n=10 for 4H

control, n=10 for 6H control, and n=12 for 8H control). To prevent overcrowding during the treatment protocol the 1280, 1920, and 2560 J/cm^2 treatments were performed separately with an equal number of control mice (n=10 for 4H control, n=10 for 6H control, and n=12 for 8H control). The mice and tumors were assessed for humane outcomes (e.g., tumor rupturing, bleeding, immobilization) before, during, and after RL treatments. Daily irradiations continued until a single mouse required euthanization for a humane endpoint, at which point, all control and RL-treated mice were euthanized (day 13 for 1280 and 1920 J/cm^2, day 15 for 2560 J/cm^2). Mice and melanoma tumor dimensions were tracked daily and photographed with a Nikon D3500 following euthanization.

Quantification of Melanoma Growth

Tumors were excised from euthanized mice and measured in three dimensions to confirm the calculated volume. The overlying skin was preserved *in situ* for histologic analysis. Tumor volume was calculated from the excised tumor using the following formula that includes a depth parameter (24):

$$Volume = \frac{\pi}{6} Lenght \times Width \times Depth$$

Tissue Histology

Following euthanization, tumors were excised and fixed in 10% formalin. The fixed skin and tumor samples with *in situ* skin were sent to Histowiz (Brooklyn, NY) for processing according to a standard operating procedure and fully automated workflow (**Supplemental Methods**).

Quantification of IHC Staining Intensity

Whole tumor and skin section images were imported into the HALO software database (Indica Labs). Quantitative biomarkers were analyzed using Multiplex IHC, area quantification, and tissue classifier modules. IHC staining was indexed to the viable tumor or skin area for all analyses. A dermatopathologist (EH) confirmed the validity of immunohistochemical staining.

Data Analysis

Data analysis was performed for all paired assays (RL to matched controls) using a two-tailed T-test. Analysis of Variance (ANOVA) was used to compare experiments with multiple comparison groups. Statistical significance was determined with a P-value of less than 0.05. GraphPad software was used for statistical testing and figure generation.

RESULTS

RL Phototherapy of Melanoma Decreases Cell Count by Inhibiting Proliferation and Increasing Cell Apoptosis

We have demonstrated that 320 and 640 J/cm^2 RL decreases human dermal fibroblasts (HDFs) proliferation and modulates the expression of fibrotic and oxidative stress pathways (19, 25, 26).

Other researchers have found that blue light, but not RL at fluences up to 360 J/cm^2, decreased B16F10 melanoma survival and proliferation (27–29). Low fluence RL has had variable effects (i.e., no changes, increases, or decreases) on survival in other cancer models (e.g., lung cancer, squamous cell carcinoma, glioblastoma, and breast cancer) (29–31). Thus, unpigmented (A375) and pigmented (MNT-1 and B16F10) melanoma cells were irradiated with 640 and 1280 J/cm^2 RL to determine whether higher fluences may achieve therapeutic outcomes. At 48 hours following irradiation, there was a dose-dependent decrease in A375, MNT-1, and B16F10 cell counts as measured by crystal violet staining intensity (**Figures 1A–C**). The results were confirmed using a hemocytometer at 48 hours in A375 cells treated with 640 and 1280 J/cm^2 (**Figures 1D,E**). At 48 hours, 1280 J/cm^2 significantly increased cell death, while 640 J/cm^2 RL did not (**Figure 1F**).

To determine whether increases in cell death were due to apoptosis, A375, MNT-1, and B16F10 cells were irradiated with RL and analyzed using annexin-V and 7-Aminoactinomycin D (7-AAD) flow cytometry (**Figures 2A–C**) (32, 33). At 24 hours post-irradiation, 1280 J/cm^2 (but not 640 J/cm^2) resulted in a significant increase in apoptosis compared to control. Representative annexin-V and 7-AAD flow plots are shown in **Figure 2D**.
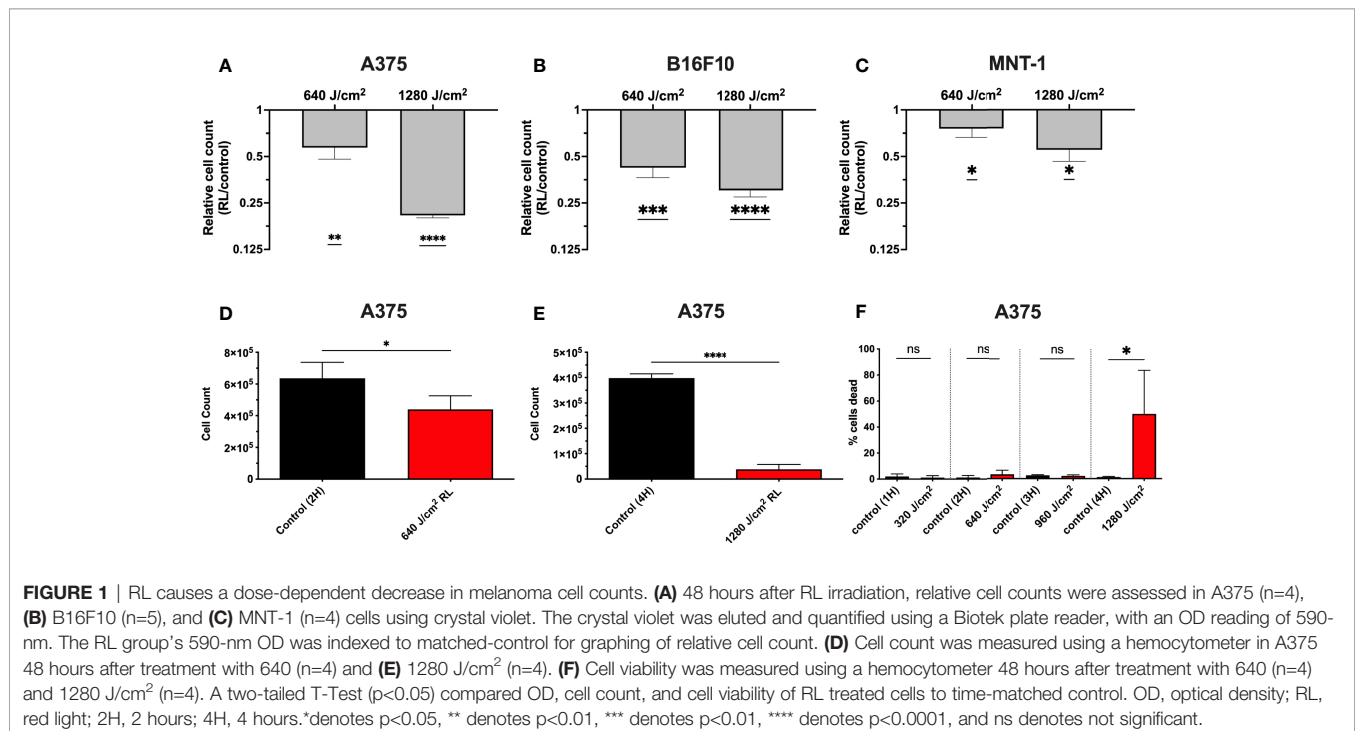
We tested whether RL regulates the cell cycle as 640 J/cm^2 decreased cell count without increasing cell death. At 24 hours post-irradiation, 640 and 1280 J/cm^2 RL significantly decreased the percentage of A375 cells in S-phase and increased the percentage in $G_{0/1}$ (**Figures 2D**). In MNT-1 cells, 1280 J/cm^2 significantly decreased the percentage of cells in the S-phase and increased the percentage in the $G_{0/1}$-phase (**Figure 2E**). MNT-1

cells irradiated with 640 J/cm^2 had decreased, but not significant, alterations in S or $G_{0/1}$ (**Figure 2F**). Representative PI flow plots are shown in **Figure 2G**.

Regulation of the Cell Cycle and Apoptosis Was Associated With Increased p53 Phosphorylation

As RL may increase cell apoptosis and regulate the cell cycle, p53 expression and phosphorylation were measured in B16F10 and A375 cells using western blot. Phosphorylation of p53 at Ser15 promotes the dissociation of p53 from MDM2 (HDM2), apoptosis activation, and cell cycle regulation (34, 35). B16F10 and A375 were examined as these cell lines are wild-type for p53 (36). Protein from A375 and B16F10 cells was collected 24 hours following irradiation. In A375 cells, 640 and 1280 J/cm^2 increased p53 by 1.2 to 1.6 fold (**Figure 3A**). In B16F10 cells, 640 and 1280 J/cm2 RL both increased total p53 by 1.3-fold (**Figures 3B**). Phosphorylated p53 increased by 1.8-fold and 2.7-fold in 640 and 1280 J/cm^2 treated A375 cells and by 1.5-fold and 2.7-fold in 640 and 1280 J/cm^2 treated B16F10 cells (**Figures 3C, D**).

Next, p21 expression was measured as p53 phosphorylation increases the transcription of *CDKN1*, the gene for p21 (an inhibitor of the cell cycle progression) (34, 37). In A375 cells, there was a dose-dependent increase in p21 expression following RL irradiation (**Figure 3E**). However, in B16F10 cells, p21 expression increased following 640 J/cm^2 RL but decreased after 1280 J/cm^2 RL (**Figure 3F**). Knockdown of p21 with siRNA transfection did not restore the cell count of 640 J/cm^2 RL treated A375 cells (**Supplemental Figure 3**). As a result, p21 knockdown is unlikely to be solely responsible for RL-mediated anti-proliferative effects.

FIGURE 1 | RL causes a dose-dependent decrease in melanoma cell counts. **(A)** 48 hours after RL irradiation, relative cell counts were assessed in A375 (n=4), **(B)** B16F10 (n=5), and **(C)** MNT-1 (n=4) cells using crystal violet. The crystal violet was eluted and quantified using a Biotek plate reader, with an OD reading of 590-nm. The RL group's 590-nm OD was indexed to matched-control for graphing of relative cell count. **(D)** Cell count was measured using a hemocytometer in A375 48 hours after treatment with 640 (n=4) and **(E)** 1280 J/cm^2 (n=4). **(F)** Cell viability was measured using a hemocytometer 48 hours after treatment with 640 (n=4) and 1280 J/cm^2 (n=4). A two-tailed T-Test (p<0.05) compared OD, cell count, and cell viability of RL treated cells to time-matched control. OD, optical density; RL, red light; 2H, 2 hours; 4H, 4 hours.*denotes p<0.05, ** denotes p<0.01, *** denotes p<0.01, **** denotes p<0.0001, and ns denotes not significant.
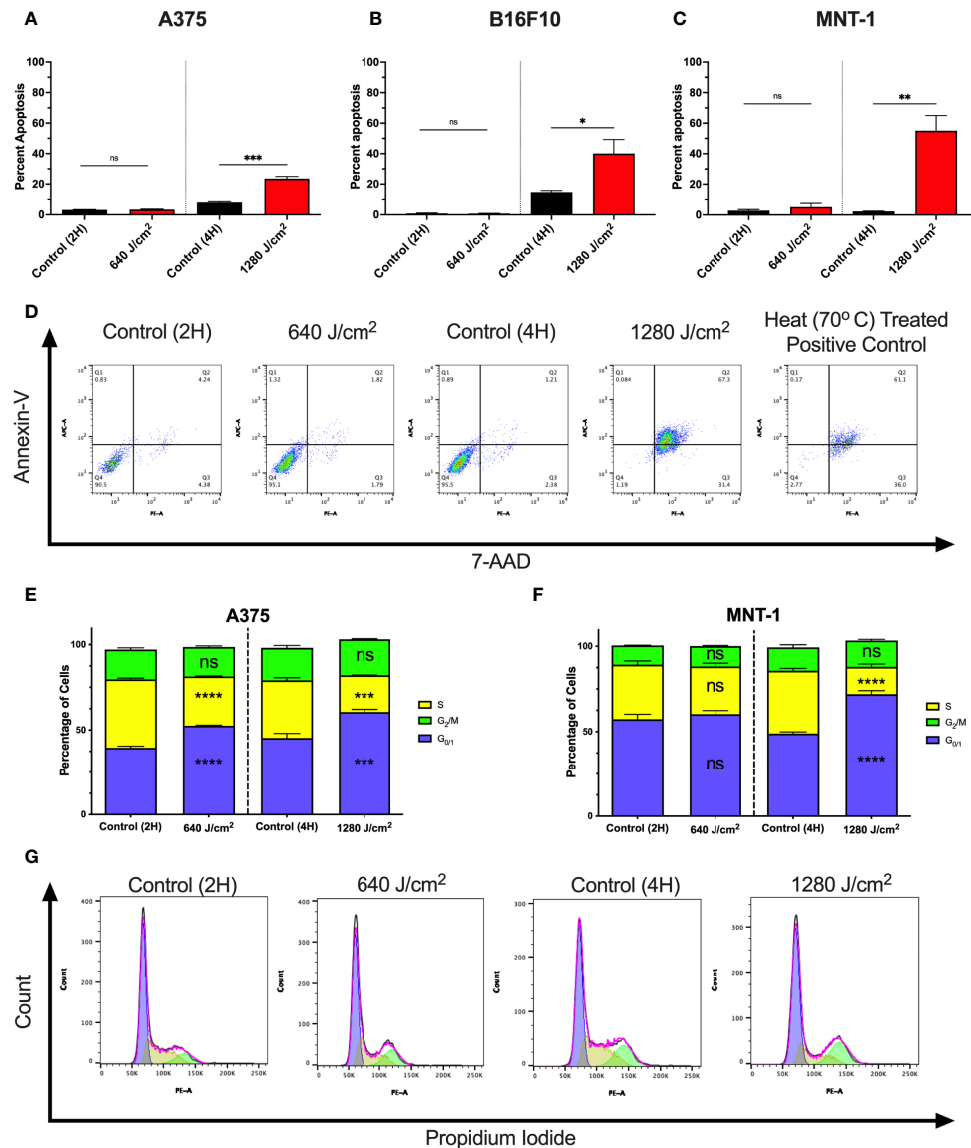
FIGURE 2 | RL increases cell death and alters the cell cycle. **(A)** Cell death was confirmed in A375 (n=3), **(B)** B16F10 (n=5), and **(C)** MNT-1 (n=5) melanoma cells using annexin-v and 7-AAD flow cytometry. **(D)** Representative flow plots for annexin-V and 7-AAD. A heat-treated positive control (70°C) was used for gating. **(E)** Cell cycle progression was assessed using PI flow cytometry in A375 (n=3) and **(F)** MNT-1 (n=3) cells. The percentage of cells in each phase was modeled using the Watson pragmatic model in FlowJo. **(G)** Representative cell cycle phase histograms from the A375 cell line. Apoptosis and cell cycle distribution compared RL and time-matched control groups using a two-tailed T-Test (p<0.05). 2H, 2 hours; 4H, 4 hours; PI, propidium iodide; 7-AAD, 7-Aminoactinomycin D; and RL, red light. *denotes p<0.05, ** denotes p<0.01, *** denotes p<0.001, **** denotes p<0.0001, and ns denotes ns.

RL Phototherapy Increases ROS Generation but Does Not Induce the Formation of Cyclobutane Pyrimidine Dimers (CPDs)

p53 may be activated by cellular stress such as DNA damage or directly by ROS. Photobiomodulation increases ROS production *via* activation of electron transport and mitochondrial dysfunction (9, 38). We have previously demonstrated that 640 J/cm^2 RL increased intracellular ROS in HDFs (19). Immediately

after 640 and 1280 J/cm^2 RL (0 hours), the cells were treated with dihydrorhodamine-123 (DHR-123) to measure intracellular ROS. 640 and 1280 J/cm^2 increased intracellular ROS in A375 and MNT-1 (**Figures 4A, C**). In B16F10 cells, 1280 J/cm^2 RL increases intracellular ROS production (**Figure 4B**).

To confirm whether increases in ROS were mechanistically linked to decreases in cell proliferation, we pretreated A375 and B16F10 cells with an antioxidant, n-acetylcysteine (NAC), and irradiated cells with 640 J/cm^2 RL. NAC sequesters ROS and has
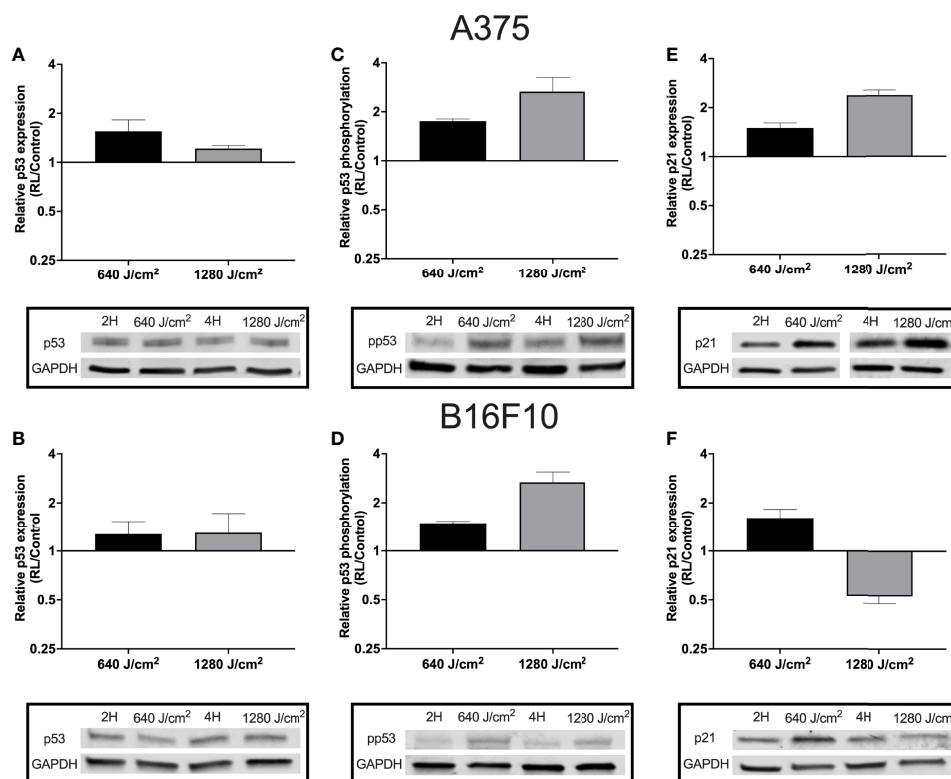
FIGURE 3 | RL increases p53 expression and phosphorylation. Protein was collected from A375 and B16F10 cells at 24 hours following irradiations with 640 and 1280 J/cm2. Relative expression of p53 in **(A)** A375 and **(B)** B16F10. Isolated protein from A375 cells treated with 640 and 1280 J/cm2 RL or control was probed with p53 antibodies twice (n=2) and six times (n=6), respectively. Isolated protein from B16F10 cells treated with 640 and 1280 J/cm2 RL or control was probed with p53 antibodies three times (n=3) and twice (n=2). **(C)** p53 phosphorylation was measured in A375 and **(D)** B16F10 cells. In A375 cells, 640 and 1280 J/cm^2 treated samples were run five-times (n=5) and three times (n=3), respectively. In B16F10 cells, 640 and 1280 J/cm^2 treated samples were analyzed with phosphorylated p53 antibodies twice (n=2) and five times (n=5). **(E)** p21 expression in A375 and **(F)** B16F10 cells following irradiation with 640 and 1280 J/cm^2 RL. In A375 cells, 640 and 1280 J/cm^2 treated samples were run five-times (n=5) and twice (n=2). In B16F10 cells, 640 and 1280 J/cm^2 treated samples were run three-times (n=3) and twice (n=2). 2H, 2 hour control; 4H, 4 hour control; 640, 640 J/cm^2; 1280, 1280 J/cm^2; ns, not significant; and RL, Red light.

previously been used in melanoma research to study oxidative stress (12, 39). In A375, pretreatment with 5 mM NAC prevented 640 J/cm^2 RL mediated decreases in cell count (**Figure 4D**). In B16F10 cells, 0.25 mM to 7.5 mM NAC prevented decreases in cell count following RL phototherapy (**Figure 4E**).

ROS from 60 J/cm^2 of UVA has been shown to interact with melanin and induce CPDs within 3-hours post-irradiation *via* chemiexcitation (40). Others have found that 5 J/cm^2 RL did not cause CPDs in MNT-1 and B16F10 cells (41). CPDs in DNA were measured from RL irradiated MNT-1 and B16F10 cells (**Figures 4F, G**). Neither 640 nor 1280 J/cm^2 RL induced DNA damage by 3 hours post-irradiation.

RL at Fluences up to 2560 J/cm^2 Is Safe in Mice

To translate *in vitro* findings to clinical regimens, the safety of RL phototherapy was first assessed in normal C57BL/6 mice (i.e., without melanoma inoculation). Daily 1280, 1920, and 2560 J/cm^2 RL sessions were administered. The mice were awake and unrestrained during RL irradiations to prevent stress-related

immunosuppression (42, 43). Higher fluences were tested *in vivo* as mice often require higher therapeutic drug doses than *in vitro* cell culture and human patients due to differences in body physiology and metabolism (44). Interspecies allometric dosing conversion equations exist for pharmaceuticals but are not available for phototherapeutic interventions (44). After 15 days of treatment, the RL-treated mice had no increase in rectal temperature, and the skin was non-inflamed and non-erythematous compared to non-treated mice (**Figure 5A**).

RL Phototherapy Inhibited Melanoma Tumor Growth *In Vivo*

As RL was safe in normal mouse skin, C57BL/6 mice were intradermally injected with 3×10^5 B16F10 cells to investigate the efficacy of RL phototherapy for melanoma (45). On day three following melanoma inoculation, the mice were randomly sorted into RL treated and control groups (45). There was no difference in tumor surface area between the RL and control groups before initiating treatment (**Supplemental Figure 4**). Mice were then irradiated with 1280, 1920, and 2560 J/cm^2 daily until humane
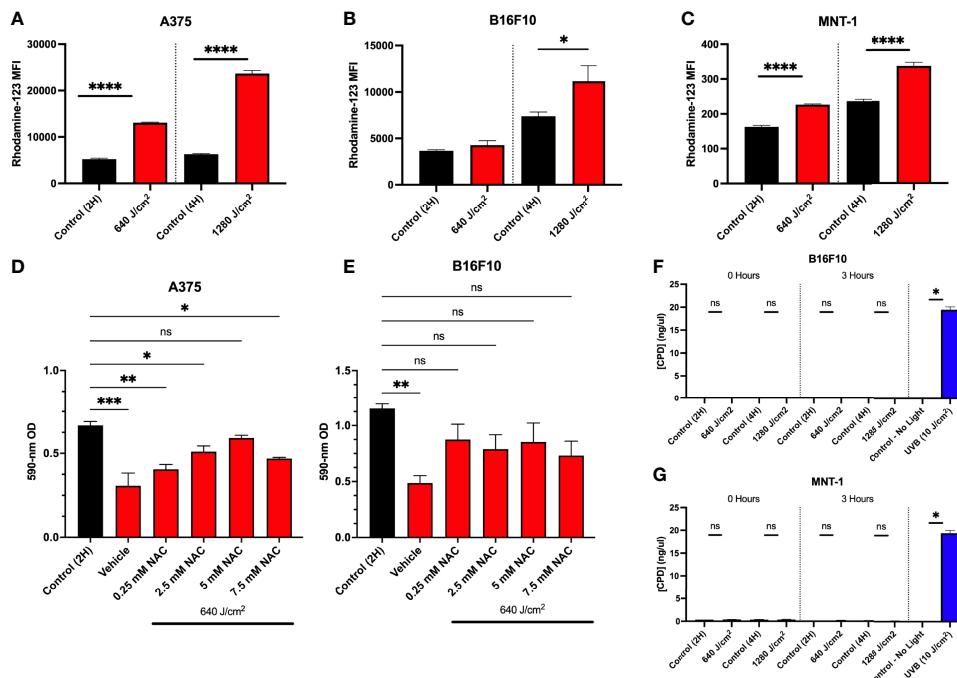
FIGURE 4 | Increases in ROS due to RL decrease cell proliferation. **(A)** A375 (n=3), **(B)** B16F10 (n=5), and **(C)** MNT-1 (n=4) cells were irradiated with 640 and 1280 J/cm² RL, and rhodamine-123 MFI was assessed at 0 hours post-treatment using flow cytometry. **(D)** A375 (n=4) and **(E)** B16F10 (n=5) cells were pretreated with 0.25 to 7.5 mM NAC and irradiated with 640 J/cm² RL. Cell count was assessed by measuring cell staining intensity with crystal violet 48 hours after irradiation. **(G)** B16F10 and **(F)** MNT-1 cells were irradiated with 640 to 1280 J/cm² RL or UVB (10 J/cm²). DNA was collected at 0 and 3 hours post-irradiation and analyzed for CPDs using ELISA. RL and control MFI and CPD concentration for 640 and 1280 J/cm² RL was compared using a two-tailed T-test (p<0.05). ANOVA was used to compare RL and NAC treated groups to control. Cell count was assessed by measuring cell staining intensity with crystal violet 48 hours after NAC. Ordinary one-way ANOVA (p<0.05) compared NAC pretreatments and control. Dunnett's *post-hoc* testing compared the mean of every RL group to control. 2H, 2 hour; 4H, 4 hour; UVB, ultraviolet B; NAC, n-acetylcysteine; OD, optical density. *denotes p<0.05, ** denotes p<0.01, *** denotes p<0.001, **** denotes p<0.0001, ns and denotes not significant.

endpoints (i.e., the tumor bled or ruptured) (45). RL caused a dose-dependent decrease in tumor volume (**Figures 5B–D**). In the 2560 J/cm² RL-treated group, tumor volumes were significantly smaller than the control (p<0.05, **Figure 5D**). Figure E shows intact tumors on the backs of 8 control and 2560 J/cm² RL-treated mice. Immunohistochemistry (IHC) demonstrated non-significant decreases in Ki-67+(p=0.19, n=8) and increases in p53+ (p=0.28, n=5) in the 2560 J/cm² RL group compared to the control (**Figures 5F–H**).

RL Increases the Infiltration of CD103+ Dendritic Cells in the Peritumoral Skin

As the C57BL/6 mice used in these experiments were immunocompetent, we assessed the effects of RL phototherapy on dermal and tumor immune infiltration. Tumor immune microenvironment can substantially affect patient prognosis (46–49). IHC was performed with excised tumors and peritumoral skin using immune markers for lymphocytes (CD3, CD4, CD8, FoxP3), dendritic cells (CD103), macrophages (CD68), and neutrophils (Ly6G).

Control and RL-treated tumors were negligibly stained for all immune markers, suggesting the exclusion of immune cells from the tumor (data not shown). The peritumor skin stained positively

for CD103, CD68, CD3, and CD4 (**Figure 6**) but negligibly for CD8, Foxp3, and Ly6G (data not shown). 2560 J/cm² RL significantly increased CD103+ expression in peritumoral skin (**Figure 6A**). 2560 J/cm² RL increased CD68+ dermal staining, but not significantly (**Figure 6B**). CD4, but not CD3, expression increased in response to RL phototherapy (**Figures 6C, D**). IHC for CD103, CD68, CD3, and CD4 was also assessed in non-tumor mice to determine the effects of RL on immune function without cancer (**Supplemental Figure 5**). RL caused a significant decrease in CD103 expression at 1280-1920 J/cm² and a modest dose-dependent increase in CD4+ expression in normal mouse skin.

DISCUSSION

Herein, we investigated the anti-tumor effects of RL phototherapy using *in vitro* and vivo models of melanoma. The ultimate goal of our RL preclinical experiments was to demonstrate therapeutic proof-of-concept and identify underlying mechanisms of action.

In vitro, 640 and 1280 J/cm² RL phototherapy decreased cell proliferation, while 1280 J/cm² RL also increased cell apoptosis. Cell cycle regulation and apoptosis were associated with p53 activation and increased ROS generation. Activating p53 may be a beneficial
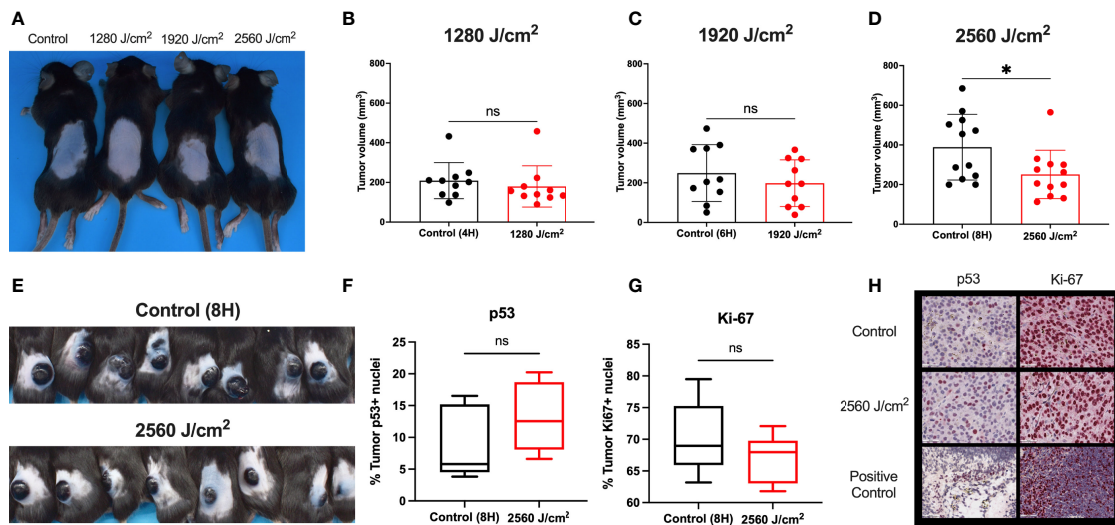
FIGURE 5 | RL safety and efficacy. **(A)** C57BL/6 mice without tumors were treated with RL at 1280, 1920, and 2560 J/cm^2 for 15 days (n=3). Mice had no increase in rectal temperature, and the skin was non-inflamed and non-erythematous compared to non-RL treated mice. **(B)** C57BL/6 Mice were injected with 3 x 10^5 melanoma cells and irradiated daily with 1280 J/cm^2 (n=10), **(C)** 1920 J/cm^2 (n=10), and **(D)** 2650 J/cm^2 RL (n=12). Volume was calculated using the formula Volume = 0.52 x length x width x depth. **(E)** Representative mice with tumors (n=8) in the control group and 2560 J/cm^2 RL group on day 15. **(F)** Quantification of p53+ (n=5) and **(G)** Ki-67+ (n=5) staining nuclei in from control (8H) and 2560 J/cm^2 treated tumors. Quantification of staining was performed using Indica HALO software. **(H)** Representative images of p53+ and Ki-67+ staining in tumors. Cephalic (embryonic day 14) and spleen positive control sections are provided for p53 and Ki-67. Excised tumor volumes and IHC staining intensity for RL-treated mice were compared to matched controls by a two-tailed T-test (p<0.05). *denotes p<0.05. ns denotes not significant.

mechanism as approximately 80-90% of melanomas are wild-type for p53 (50, 51). Wild-type p53 can regulate cell cycle checkpoint progress and induce apoptosis in response to oxidative stress or DNA damage repair pathways (52, 53). In HDFs, 640 J/cm^2 similarly did not increase p21 expression, despite increasing p53 phosphorylation (54). Additionally, suprathreshold oxidative stress has been shown to inhibit melanoma growth and promote apoptosis independently (14). Pretreatment of melanoma cells with NAC inhibited the anti-proliferative effects of RL phototherapy in melanoma cells. Others have similarly found that antioxidants, including NAC, increased melanoma metastasis in mouse models (12, 39). Therefore, increased oxidative stress may be a therapeutically beneficial mechanism of action (55).

We then translated RL phototherapy protocols to animal models after demonstrating anti-tumor effects *in vitro*. B16F10 melanoma cells were used for *in vivo* protocols as the tumors grow rapidly and with consistent kinetics (45, 56). As such, multiple RL treatment fluences (i.e., 1280, 1920, and 2560 J/cm^2) could be screened for potential efficacy. Additionally, C57BL/6 mice injected with B16F10 are immunocompetent, thus allowing for the assessment of immune function. In mice, irradiation of 2560 J/cm^2 for up to 13 days decreased B16F10 melanoma tumor size compared to control. These results differ from previous studies in which three days of 1050 J/cm^2 RL from an In-Ga-Al-AsP laser (660-nm) increased murine melanoma tumor growth (57). As a result, higher fluences of RL and longitudinal treatment protocols may be necessary for clinical translation. Future clinical trials are necessary to convert RL phototherapy dosing regimens from cell culture and mice to patients and evaluate the efficacy of different phototherapy regimens, including photobiomodulation, photothermal therapy, and photodynamic therapy (58, 59).

To determine whether RL may be combined with existing pharmaceutical approaches, including immune checkpoint inhibitors, we investigated the effects of RL phototherapy on tumor immune responses. RL increased the expression of CD103+, a marker of migratory dendritic cells that enhance antigen presentation to cytotoxic T-cells in the lymph nodes (60–62). CD103+ expression is linked to favorable immune microenvironments, improved prognoses, prevention of metastasis, and responsiveness to PD-1/PD-1L inhibitor therapy (60–62). CD4 expression, classically a helper T-cell marker, was similarly increased following RL phototherapy. However, CD4 is also non-specifically expressed on macrophages and dendritic cells, and flow cytometry is necessary to fully characterize the immune cell populations and T-cell infiltration (63). Other researchers have also examined the role of immune activity in phototherapy (64, 65). Ottaviani et al. used RL phototherapy to decrease tumor volume and increase the expression of type I interferons (65, 66). Type I interferons are involved with immune surveillance, dendritic cell maturation, and inflammatory responses (65, 66). Together, previous research and our results suggest that RL may activate systemic immune responses in melanoma mouse models and facilitate a therapeutic immune niche. Therefore, RL phototherapy may be synergistically combined with current melanoma therapies for the benefit of patients.

Our research on RL phototherapy has strengths and weaknesses. One strength is that we utilized multiple *in vitro* and *in vivo* protocols to confirm laboratory findings. Another strength is that the culture media and mouse core body temperatures were
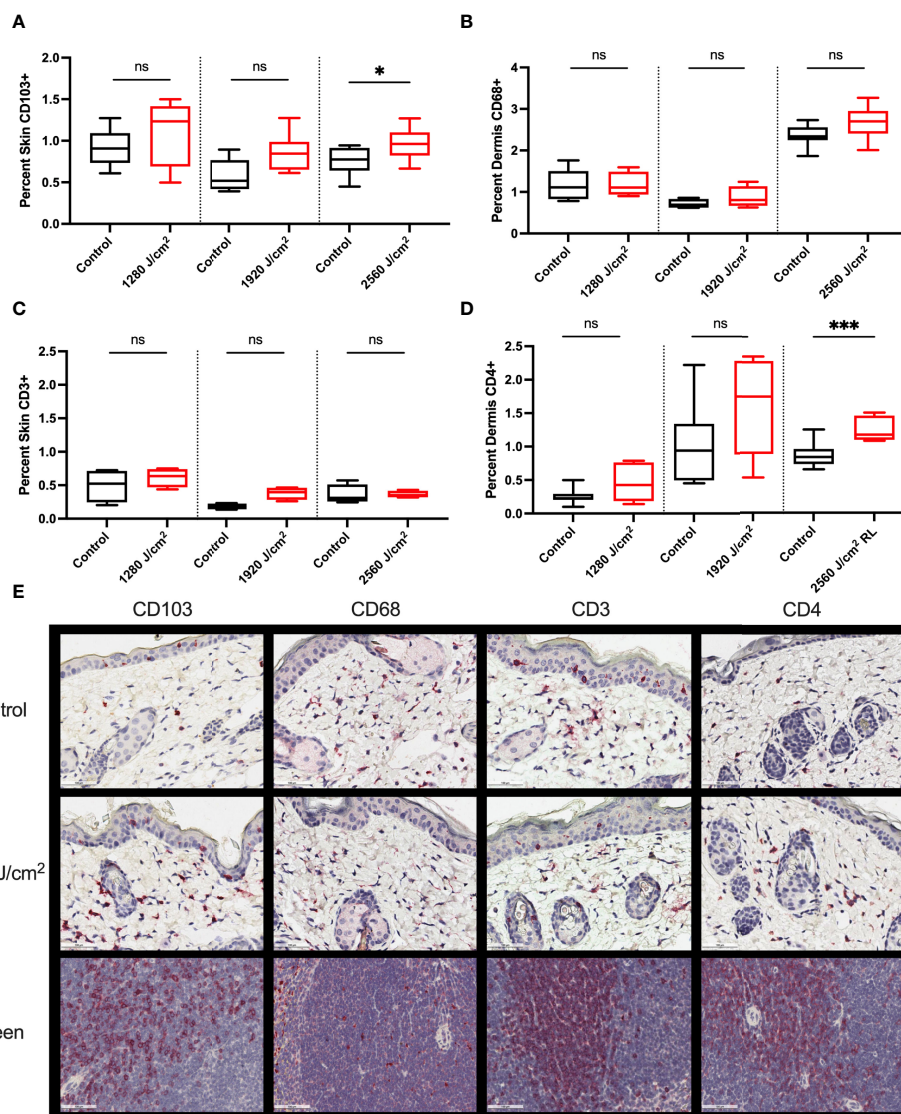
FIGURE 6 | RL increases the expression of immunocyte markers. **(A)** Quantification of CD103 (n=8), **(B)** CD68 (n=5 for 1280 J/cm², n=4 for 1920 J/cm², n=8 for 2560 J/cm²), **(C)** CD3 (n=4), and **(D)** CD4 (n=8) staining in the peritumoral dermis or skin from 1280, 1920, and 2560 J/cm² RL-treated and control C57BL/6 mice injected with B16F10 cells (two-tailed T-Test, p<0.05). **(E)** Representative IHC for CD103, CD68, CD3, and CD4 positive staining peritumoral dermis and skin. The staining intensity of each marker was indexed to the total skin or dermal area for each section. Spleen positive control tissue is provided. Staining was quantified using Indica HALO software and compared to total skin or dermal area. * denotes p<0.05, *** denotes p<0.001, ns denotes not significant.

carefully maintained at physiological levels during irradiations. Controlling temperature is essential as increased heat (40°C and above) may independently lead to decreased cell viability, increased ROS generation, G_1 cell cycle arrest, membrane denaturation, and coagulative necrosis (15, 67–70). 450 J/cm² RL (650-nm) has been shown to cause membrane protein denaturation in red blood cells (70). Three human studies by our research team tested the safety of LED RL in patients, and fluences of 320-480 J/cm² (treatment duration of 1-1.5 hours) caused occasional erythema and blistering, respectively, in patients without the use of a cooling device (71, 72). In mice, fluences up to 2560 J/cm² of

RL with air-conditioning did not induce erythema, blistering, or ulceration in non-tumor mouse skin. Cooling devices are often incorporated in laser systems, and future clinical trials could test higher fluences with temperature regulation (73). However, photothermal reactions and inefficient energy transfer may increase intracellular temperature despite external cooling (15, 68, 70). A potential weakness of our mouse protocols is that the mice were awake and unrestrained to prevent immunosuppression. Therefore, the mice were able to huddle up and turn away from the light, which resulted in variability in treatment fluence depending on individual mouse behavior (42, 43). In future

experiments, higher power density LEDs or lasers may be tested to reduce total treatment duration.

RL represents a potentially promising approach for melanoma therapy, as RL is inexpensive, noninvasive, easily combined with existing melanoma pharmacologic treatments, and associated with low morbidity and no known mortality. Additionally, RL can be made available for home use to augment existing melanoma therapies under the guidance of a physician. Clinical studies have demonstrated that patients can safely use LED devices at home (74). Clinical translation for melanoma therapy could quickly follow safety and efficacy demonstration in phase I-III clinical trials. We anticipate that soon, it may be possible for patients to use home RL phototherapy to augment therapy for cutaneous melanoma metastasis, empowering patients to participate in their cancer treatment.

DATA AVAILABILITY STATEMENT

The raw data supporting the conclusions of this article will be made available by the authors, without undue reservation.

ETHICS STATEMENT

The animal study was reviewed and approved by SUNY Downstate IACUC.

AUTHOR CONTRIBUTIONS

EA investigated, performed data analysis, data curated, and wrote the original draft. AH investigated and performed data analysis. JW investigated and performed data analysis. MC investigated and performed data analysis. EH performed data analysis and reviewed and edited. JM reviewed and edited and provided resources. EM reviewed and edited and provided resources. JJ reviewed and edited, acquired funding, supervised, performed projected administration, and provided resources. All authors contributed to the article and approved the submitted version.

FUNDING

SUPPLEMENTARY MATERIAL

The Supplementary Material for this article can be found online at: https://www.frontiersin.org/articles/10.3389/fonc.2022.928484/full#supplementary-material

REFERENCES

1. Glazer AM, Winkelmann RR, Farberg AS, Rigel DS. Analysis of Trends in US Melanoma Incidence and Mortality. *JAMA Dermatol* (2017) 153(2):225–6. doi: 10.1001/jamadermatol.2016.4512

2. Apalla Z, Lallas A, Sotiriou E, Lazaridou E, Ioannides D. Epidemiological Trends in Skin Cancer. *Dermatol Pract conceptual* (2017) 7(2):1. doi: 10.5826/dpc.0702a01

3. Siegel RL, Miller KD, Goding Sauer A, Fedewa SA, Butterly LF, Anderson JC, et al. Colorectal Cancer Statistics, 2020. *CA: Cancer J Clin* (2020) 70(3):145–64. doi: 10.3322/caac.21601

4. Domingues B, Lopes JM, Soares P, Pópulo H. Melanoma Treatment in Review. *ImmunoTargets Ther* (2018) 7:35–49. doi: 10.2147/ITT.S134842

5. Schadendorf D, van Akkooi AC, Berking C, Griewank KG, Gutzmer R, Hauschild A, et al. Melanoma. *Lancet* (2018) 392(10151):971–84. doi: 10.1016/S0140-6736(18)31559-9

6. Michielin O, Atkins MB, Koon HB, Dummer R, Ascierto PA. Evolving Impact of Long-Term Survival Results on Metastatic Melanoma Treatment. *J ImmunoTherapy Cancer* (2020) 8(2):e000948. doi: 10.1136/jitc-2020-000948

7. Chen L, Douglass J, Kleinberg L, Ye X, Marciscano AE, Forde PM, et al. Concurrent Immune Checkpoint Inhibitors and Stereotactic Radiosurgery for Brain Metastases in non-Small Cell Lung Cancer, Melanoma, and Renal Cell Carcinoma. *Int J Radiat Oncol Biol Physics* (2018) 100(4):916–25. doi: 10.1016/j.ijrobp.2017.11.041

8. Ahmed KA, Kim S, Harrison LB. Novel Opportunities to Use Radiation Therapy With Immune Checkpoint Inhibitors for Melanoma Management. *Surg Oncol Clinics* (2017) 26(3):515–29. doi: 10.1016/j.soc.2017.01.007

9. de Freitas LF, Hamblin MR. Proposed Mechanisms of Photobiomodulation or Low-Level Light Therapy. *IEEE J Sel Top Quantum Electron* (2016) 22 (3):348–64. doi: 10.1109/JSTQE.2016.2561201

10. Rupel K, Zupin L, Colliva A, Kamada A, Poropat A, Ottaviani G, et al. Photobiomodulation at Multiple Wavelengths Differentially Modulates Oxidative Stress In Vitro and *In Vivo*. *Oxid Med Cell Longevity* (2018) 2018. doi: 10.1155/2018/6510159

11. Zein R, Selting W, Hamblin MR. Review of Light Parameters and Photobiomodulation Efficacy: Dive Into Complexity. *J Biomed Optics* (2018) 23(12):120901. doi: 10.1117/1.JBO.23.12.120901

12. Piskounova E, Agathocleous M, Murphy MM, Murphy MM, Hu Z, Huddlestun SE, Zhao Z, et al. Oxidative Stress Inhibits Distant Metastasis by Human Melanoma Cells. *Nature* (2015) 527(7577):186–91. doi: 10.1038/nature15726

13. Perillo B, Di Donato M, Pezone A, Di Zazzo E, Giovannelli P, Galasso G, et al. ROS in Cancer Therapy: The Bright Side of the Moon. *Exp Mol Med* (2020) 52 (2):192–203. doi: 10.1038/s12276-020-0384-2

14. Trachootham D, Alexandre J, Huang P. Targeting Cancer Cells by ROS-Mediated Mechanisms: A Radical Therapeutic Approach? *Nat Rev Drug Discov* (2009) 8(7):579–91. doi: 10.1038/nrd2803

15. Mignon C, Uzunbajakava N, Raafs B, Botchkareva NV, Tobin DJ. Photobiomodulation of Human Dermal Fibroblasts *In Vitro*: Decisive Role of Cell Culture Conditions and Treatment Protocols on Experimental Outcome. *Sci Rep* (2017) 7(1):1–14. doi: 10.1038/s41598-017-02802-0

16. Lewinska A, Wnuk M, Slota E, Bartosz G. Total Anti-Oxidant Capacity of Cell Culture Media. *Clin Exp Pharmacol Physiol* (2007) 34(8):781–6. doi: 10.1111/j.1440-1681.2007.04637.x

17. Feoktistova M, Geserick P, Leverkus M. Crystal Violet Assay for Determining Viability of Cultured Cells. *Cold Spring Harbor Protoc* (2016) 2016(4):pdb.prot087379. doi: 10.1101/pdb.prot087379

18. Chowdhury KD, Sarkar A, Chatterjee S, Patra D, Sengupta D, Banerjee S, et al. Cathepsin B Mediated Scramblase Activation Triggers Cytotoxicity and Cell Cycle Arrest by Andrographolide to Overcome Cellular Resistance in Cisplatin Resistant Human Hepatocellular Carcinoma HepG2 Cells. *Environ Toxicol Pharmacol* (2019) 68:120–32. doi: 10.1016/j.etap.2019.03.003

19. Mamalis A, Koo E, Garcha M, Murphy WJ, Isseroff RR, Jagdeo J. High Fluence Light Emitting Diode-Generated Red Light Modulates Characteristics Associated With Skin Fibrosis. *J Biophotonics* (2016) 9(11-12):1167–79. doi: 10.1002/jbio.201600059

20. Crowley LC, Marfell BJ, Scott AP, Waterhouse NJ. Quantitation of Apoptosis and Necrosis by Annexin V Binding, Propidium Iodide Uptake, and Flow

Cytometry. *Cold Spring Harbor Protoc* (2016) 2016(11):pdb. prot087288. doi: 10.1101/pdb.prot087288

21. Riccardi C, Nicoletti I. Analysis of Apoptosis by Propidium Iodide Staining and Flow Cytometry. *Nat Protoc* (2006) 1(3):1458–61. doi: 10.1038/nprot.2006.238

22. Zimmermann M, Meyer N. Annexin V/7-AAD Staining in Keratinocytes. In: *Mammalian Cell Viability*. Totowa, New Jersey: Humana Press (2011). p. 57–63.

23. Mamalis A, Jagdeo J. Light-Emitting Diode-Generated Red Light Inhibits Keloid Fibroblast Proliferation. *Dermatol Surg* (2015) 41(1):35–9. doi: 10.1097/01.DSS.0000452650.06765.51

24. Tomayko MM, Reynolds CP. Determination of Subcutaneous Tumor Size in Athymic (Nude) Mice. *Cancer Chemotherapy Pharmacol* (1989) 24(3):148–54. doi: 10.1007/BF00300234

25. Lev-Tov H, Mamalis A, Brody N, Siegel D, Jagdeo J. Inhibition of Fibroblast Proliferation *In Vitro* Using Red Light-Emitting Diodes. *Dermatol Surg* (2013) 39(8):1167–70. doi: 10.1111/dsu.12212

26. Austin E, Koo E, Merleev A, Torre D, Marusina A, Luxardi G, et al. Transcriptome Analysis of Human Dermal Fibroblasts Following Red Light Phototherapy. *Sci Rep* (2021) 11(1):7315. doi: 10.1038/s41598-021-86623-2

27. Sato K, Minai Y, Watanabe H. Effect of Monochromatic Visible Light on Intracellular Superoxide Anion Production and Mitochondrial Membrane Potential of B16F1 and B16F10 Murine Melanoma Cells. *Cell Biol Int* (2013) 37(6):633–7. doi: 10.1002/cbin.10069

28. Oh P-S, Na KS, Hwang H, Jeong H-S, Lim ST, Sohn M-H, et al. Effect of Blue Light Emitting Diodes on Melanoma Cells: Involvement of Apoptotic Signaling. *J Photochem Photobiol B: Biol* (2015) 142:197–203. doi: 10.1016/j.jphotobiol.2014.12.006

29. Hopkins SL, Siewert B, Askes S, Veldhuizen P, Zwier R, Heger M, et al. An *In Vitro* Cell Irradiation Protocol for Testing Photopharmaceuticals and the Effect of Blue, Green, and Red Light on Human Cancer Cell Lines. *Photochemical Photobiological Sci* (2016) 15(5):644–53. doi: 10.1039/C5PP00424A

30. Goo H, Mo S, Park HJ, Lee MY, Ahn JC. Treatment With LEDs at a Wavelength of 642 Nm Enhances Skin Tumor Proliferation in a Mouse Model. *BioMed Opt Express* (2021) 12(9):5583–96. doi: 10.1364/BOE.427205

31. Schalch TD, Fernandes MH, Destro Rodrigues MFS, Guimarães DM, Nunes FD, Rodrigues JC, et al. Photobiomodulation is Associated With a Decrease in Cell Viability and Migration in Oral Squamous Cell Carcinoma. *Lasers Med Sci* (2019) 34(3):629–36. doi: 10.1007/s10103-018-2640-4

32. Van Engeland M, Nieland LJ, Ramaekers FC, Schutte B, Reutelingsperger CP. Annexin V-Affinity Assay: A Review on an Apoptosis Detection System Based on Phosphatidylserine Exposure. *Cytometry: J Int Soc Analytical Cytol* (1998) 31(1):1–9. doi: 10.1002/(SICI)1097-0320(19980101)31:1<1::AID-CYTO1>3.0.CO;2-R

33. Martinez MM, Reif RD, Pappas D. Detection of Apoptosis: A Review of Conventional and Novel Techniques. *Analytical Methods* (2010) 2(8):996–1004. doi: 10.1039/c0ay00247j

34. Hafner A, Bulyk ML, Jambhekar A, Lahav G. The Multiple Mechanisms That Regulate P53 Activity and Cell Fate. *Nat Rev Mol Cell Biol* (2019) 20(4):199–210. doi: 10.1038/s41580-019-0110-x

35. Shieh S-Y, Ikeda M, Taya Y, Prives C. DNA Damage-Induced Phosphorylation of P53 Alleviates Inhibition by MDM2. *Cell* (1997) 91(3):325–34. doi: 10.1016/S0092-8674(00)80416-X

36. Melnikova VO, Bolshakov SV, Walker C, Ananthaswamy HN. Genomic Alterations in Spontaneous and Carcinogen-Induced Murine Melanoma Cell Lines. *Oncogene* (2004) 23(13):2347–56. doi: 10.1038/sj.onc.1207405

37. Hume S, Dianov GL, Ramadan K. A Unified Model for the G1/S Cell Cycle Transition. *Nucleic Acids Res* (2020) 48(22):12483–501. doi: 10.1093/nar/gkaa1002

38. Hamblin MR. Mechanisms and Mitochondrial Redox Signaling in Photobiomodulation. *Photochem Photobiol* (2018) 94(2):199–212. doi: 10.1111/php.12864

39. Le Gal K, Ibrahim MX, Wiel C, Sayin VI, Akula MK, Karlsson C, et al. Antioxidants can Increase Melanoma Metastasis in Mice. *Sci Trans Med* (2015) 7(308):308re308–308re308. doi: 10.1126/scitranslmed.aad3740

40. Premi S, Wallisch S, Mano CM, Weiner AB, Bacchiocchi A, Wakamatsu K, et al. Chemiexcitation of Melanin Derivatives Induces DNA Photoproducts

Long After UV Exposure. *Science* (2015) 347(6224):842–7. doi: 10.1126/science.1256022

41. Mudambi S, Pera P, Washington D, Remenyik E, Fidrus E, Shafirstein G, et al. Photodynamic Therapy Does Not Induce Cyclobutane Pyrimidine Dimers in the Presence of Melanin. *Photodiagnosis Photodyn Ther* (2018) 22:241–4. doi: 10.1016/j.pdpdt.2018.04.018

42. Schwab CL, Fan R, Zheng Q, Myers LP, Hébert P, Pruett SB. Modeling and Predicting Stress-Induced Immunosuppression in Mice Using Blood Parameters. *Toxicol Sci* (2005) 83(1):101–13. doi: 10.1093/toxsci/kfi014

43. Nishioka K, Okano M, Ichihara Y, Ichihara N, Nishizaki K. Immunosuppressive Effect of Restraint Stress on the Initiation of Allergic Rhinitis in Mice. *Int Arch Allergy Immunol* (2005) 136(2):142–7. doi: 10.1159/000083321

44. Nair AB, Jacob S. A Simple Practice Guide for Dose Conversion Between Animals and Human. *J Basic Clin Pharm* (2016) 7(2):27–31. doi: 10.4103/0976-0105.177703

45. Overwijk WW, Restifo NP. B16 as a Mouse Model for Human Melanoma. *Curr Protoc Immunol* (2000) 39:20.1.1–20.1.29. doi: 10.1002/0471142735.im2001s39

46. Erkes DA, Cai W, Sanchez IM, Purwin TJ, Rogers C, Field CO, et al. Mutant BRAF and MEK Inhibitors Regulate the Tumor Immune Microenvironment *via* Pyroptosis. *Cancer Discov* (2020) 10(2):254–69. doi: 10.1158/2159-8290.CD-19-0672

47. Gartrell-Corrado RD, Chen AX, Rizk EM, Marks DK, Bogardus MH, Hart TD, et al. Linking Transcriptomic and Imaging Data Defines Features of a Favorable Tumor Immune Microenvironment and Identifies a Combination Biomarker for Primary Melanoma. *Cancer Res* (2020) 80(5):1078–87. doi: 10.1158/0008-5472.CAN-19-2039

48. Santarpia M, Karachaliou N. Tumor Immune Microenvironment Characterization and Response to Anti-PD-1 Therapy. *Cancer Biol Med* (2015) 12(2):74. doi: 10.7497/j.issn.2095-3941.2015.0022

49. Taube JM, Galon J, Sholl LM, Rodig SJ, Cottrell TR, Giraldo NA, et al. Implications of the Tumor Immune Microenvironment for Staging and Therapeutics. *Modern Pathol* (2018) 31(2):214–34. doi: 10.1038/modpathol.2017.156

50. Hocker T, Tsao H. Ultraviolet Radiation and Melanoma: A Systematic Review and Analysis of Reported Sequence Variants. *Hum Mutation* (2007) 28(6):578–88. doi: 10.1002/humu.20481

51. Box NF, Vukmer TO, Terzian T. Targeting P53 in Melanoma. *Pigment Cell Melanoma Res* (2014) 27(1):8–10. doi: 10.1111/pcmr.12180

52. Kastenhuber ER, Lowe SW. Putting P53 in Context. *Cell* (2017) 170(6):1062–78. doi: 10.1016/j.cell.2017.08.028

53. Kruiswijk F, Labuschagne CF, Vousden KH. P53 in Survival, Death and Metabolic Health: A Lifeguard With a Licence to Kill. *Nat Rev Mol Cell Biol* (2015) 16(7):393. doi: 10.1038/nrm4007

54. Masub N, Austin E, Huang A, Jagdeo J. High-Fluence Light Emitting Diode-Red Light Inhibits Cell Cycle Progression in Human Dermal Fibroblasts. *J Biophotonics* 2021 2020:e202000359. doi: 10.1002/jbio.202000359

55. Wittgen HG, van Kempen LC. Reactive Oxygen Species in Melanoma and its Therapeutic Implications. *Melanoma Res* (2007) 17(6):400–9. doi: 10.1097/CMR.0b013e3282f1d312

56. Alvarez E. B16 Murine Melanoma: Historical Perspective on the Development of a Solid Tumor Model. In: *Tumor Models in Cancer Research*. Totowa, NJ: Humana Press (2011). p. 79–95.

57. Frigo L, Luppi JS, Favero GM, Maria DA, Penna SC, Bjordal JM, et al. The Effect of Low-Level Laser Irradiation (In-Ga-Al-AsP-660 Nm) on Melanoma *In Vitro* and *In Vivo*. *BMC Cancer* (2009) 9(1):1–8. doi: 10.1186/1471-2407-9-404

58. Wang L, Wang L, Zhang Y, Zhao Z, Liu C, Li M, et al. LS-HB-Mediated Photodynamic Therapy Inhibits Proliferation and Induces Cell Apoptosis in Melanoma. *Mol Pharm* (2022). doi: 10.1021/acs.molpharmaceut.2c00302

59. Ma Y, Zhang Y, Li X, Li X, Zhao Y, Li M, et al. Near-Infrared II Phototherapy Induces Deep Tissue Immunogenic Cell Death and Potentiates Cancer Immunotherapy. *ACS Nano* (2019) 13(10):11967–80. doi: 10.1021/acsnano.9b06040

60. Peranzoni E, Lemoine J, Vimeux L, Feuillet V, Barrin S, Kantari-Mimoun C, et al. Macrophages Impede CD8 T Cells From Reaching Tumor Cells and Limit the Efficacy of Anti–PD-1 Treatment. *Proc Natl Acad Sci* (2018) 115(17):E4041–50. doi: 10.1073/pnas.1720948115

61. Fu C, Jiang A. Dendritic Cells and CD8 T Cell Immunity in Tumor Microenvironment. *Front Immunol* (2018) 9:3059. doi: 10.3389/fimmu.2018.03059

62. Kitamura T, Qian B-Z, Pollard JW. Immune Cell Promotion of Metastasis. *Nat Rev Immunol* (2015) 15(2):73–86. doi: 10.1038/nri3789

63. Vremec D, Pooley J, Hochrein H, Wu L, Shortman K. CD4 and CD8 Expression by Dendritic Cell Subtypes in Mouse Thymus and Spleen. *J Immunol* (2000) 164(6):2978–86. doi: 10.4049/jimmunol.164.6.2978

64. de Castro MS, Miyazawa M, Nogueira ESC, Chavasco JK, Brancaglion GA, Cerdeira CD, et al. Photobiomodulation Enhances the Th1 Immune Response of Human Monocytes. *Lasers Med Sci* (2022) 37:135–48. doi: 10.1007/s10103-020-03179-9

65. Ottaviani G, Martinelli V, Rupel K, Caronni N, Naseem A, Zandonà L, et al. Laser Therapy Inhibits Tumor Growth in Mice by Promoting Immune Surveillance and Vessel Normalization. *EBioMedicine* (2016) 11:165–72. doi: 10.1016/j.ebiom.2016.07.028

66. Zitvogel L, Galluzzi L, Kepp O, Smyth MJ, Kroemer G. Type I Interferons in Anticancer Immunity. *Nat Rev Immunol* (2015) 15(7):405–14. doi: 10.1038/nri3845

67. Garcia MP, Cavalheiro JRT, Fernandes MH. Acute and Long-Term Effects of Hyperthermia in B16-F10 Melanoma Cells. *PLoS One* (2012) 7(4):e35489. doi: 10.1371/journal.pone.0035489

68. Mundhara N, Majumder A, Panda D. Hyperthermia Induced Disruption of Mechanical Balance Leads to G1 Arrest and Senescence in Cells. *Biochem J* (2021) 478(1):179–96. doi: 10.1042/BCJ20200705

69. Cao Q, Wang W, Zhou M, Huang Q, Wen X, Zhou J, et al. Induction of Antitumor Immunity in Mice by the Combination of Nanoparticle-Based Photothermolysis and Anti-PD-1 Checkpoint Inhibition. *Nanomedicine* (2020) 25:102169. doi: 10.1016/j.nano.2020.102169

70. Al-Yasiri AY. *In Vitro* Influence of Low-Power Diode Laser Irradiation Time on Human Red Blood Cells. *Photomedicine Laser Surg* (2018) 36(5):253–7. doi: 10.1089/pho.2017.4395

71. Kurtti A, Nguyen JK, Weedon J, Mamalis A, Lai Y, Masub N, et al. Light Emitting Diode-Red Light for Reduction of Post-Surgical Scarring: Results From a Dose-Ranging, Split-Face, Randomized Controlled Trial. *J Biophotonics* (2021) 14(7):e202100073. doi: 10.1002/jbio.202100073

72. Jagdeo J, Nguyen JK, Ho D, Wang EB, Austin E, Mamalis A, et al. Safety of Light Emitting Diode-Red Light on Human Skin: Two Randomized Controlled Trials. *J Biophotonics* (2020) 13(3):e201960014. doi: 10.1002/jbio.201960014

73. Das A, Sarda A, De A. Cooling Devices in Laser Therapy. *J Cutan Aesthet Surg* (2016) 9(4):215–9. doi: 10.4103/0974-2077.197028

74. Jagdeo J, Austin E, Mamalis A, Wong C, Ho D, Siegel DM. Light-Emitting Diodes in Dermatology: A Systematic Review of Randomized Controlled Trials. *Lasers Surg Med* (2018) 50(6):613–28. doi: 10.1002/lsm.22791